Shams Ghahfarokhi, Payam; Podgornovs, Andrejs; Kallaste, Ants; Marques Cardoso, Antonio J.; Belahcen, Anouar; Vaimann, Toomas; Kudrjavtsev, Oleg; Asad, Bilal; Iqbal, Muhammad Naveed

Steady-State Thermal Modeling of Salient Pole Synchronous Generator

Published in:
Energies

DOI:
10.3390/en15249460

Published: 01/12/2022

Document Version
Publisher's PDF, also known as Version of record

energies

MDPI

Article

Steady-State Thermal Modeling of Salient Pole Synchronous Generator

Payam Shams Ghahfarokhi [1,2,3,*], Andrejs Podgornovs [1], Ants Kallaste [2], Antonio J. Marques Cardoso [3], Anouar Belahcen [4], Toomas Vaimann [2], Oleg Kudrjavtsev [5], Bilal Asad [2] and Muhammad Naveed Iqbal [2]

1 Department of Electrical Machines and Apparatus, Riga Technical University, Kaļķu iela 1, LV-1048 Riga, Latvia
2 Department of Electrical Power Engineering and Mechatronics, Tallinn University of Technology, 19086 Tallinn, Estonia
3 CISE—Electromechatronic Systems Research Centre, University of Beira Interior, P-6201-001 Covilhã, Portugal
4 Department of Electrical Engineering and Automation, Aalto University, P.O. Box 15500, FI-00076 Aalto, Finland
5 ABB Estonia, Aruküla tee 83, 75301 Jüri, Estonia
* Correspondence: payam.shams@ttu.ee

Abstract: This paper presents a practical thermal model of a synchronous generator for high-power applications. This model couples the lumped parameter thermal network and coolant network together to utilize the impact of the coolant's temperature rising over the machine. Furthermore, the advanced multi-planes technique provides a more precise and higher resolution temperature distribution of various machine sections. Therefore, the machines are divided into five planes; three belong to the active part, and two are added to model the machine's drive and non-drive end-regions. Furthermore, the paper pays special attention to describing the challenges and providing solutions to them during the heat transfer modeling and analysis. Finally, the analytical model is verified using experimental results on a synchronous generator with a salient pole rotor and an open self-ventilation (OSV) cooling system by comparing the analytical and experimental results. As a result, good correspondence between the estimated and measurement results is achieved.

Keywords: AC machines; cooling; electrical machines; lumped parameter network; coolant network; temperature measurement; thermal analysis

Citation: Shams Ghahfarokhi, P.; Podgornovs, A.; Kallaste, A.; Marques Cardoso, A.J.; Belahcen, A.; Vaimann, T.; Kudrjavtsev, O.; Asad, B.; Iqbal, M.N. Steady-State Thermal Modeling of Salient Pole Synchronous Generator. *Energies* **2022**, *15*, 9460. https://doi.org/10.3390/en15249460

Academic Editors: Gang Lei, Xin Ba and Youguang Guo

Received: 18 November 2022
Accepted: 12 December 2022
Published: 13 December 2022

1. Introduction

Today, four-pole high megawatt solid salient rotor synchronous generators are widely used as high-power machinery in industrial applications, such as the marine, renewable energy, and oil and gas sectors. These four-pole synchronous machines with solid salient pole rotors have several advantages, such as high efficiency and low noise and vibration, but they need to have excellent thermal stability [1]. Therefore, it is necessary to investigate the machine's thermal stability by simultaneously developing a thermal analysis method with electromagnetic design. The thermal modeling approach is classified into two main groups: analytical and numerical thermal methods [2–5]. Each approach has its own advantages and drawbacks. However, since the analytical approach is a rapid computing method with acceptable accuracy, this method is mainly applied to the thermal modeling of machines [6].

One of the standard cooling systems primarily implemented on high-power generators is the open self-ventilated system. This cooling technique has advantages, such as being cost-effective and a straightforward design [7]. In this system, a fan is integrated into the rotor or mounted onto the shaft to provide differential pressure to create the airflow and pass it from the air gap and various radial and axial cooling ducts embedded in the rotor and stator. Since the performance of this cooling system significantly depends on the

amount of the machine's contact surface area with coolant, the radial and axial cooling ducts are applied in the stator and rotor to increase the contact surfaces with coolant to improve heat removal [4].

Various research studies have investigated the modeling of the heat transfer and temperature distributions of OSV machines [8–11]. Most studies have implemented analytical methods by developing the lumped parameter thermal network (LPTN) based on various techniques, such as the generic cylinder element ([11–14]), which was proposed first by Mellor et al. in [15], or the multiple planes technique ([16,17]). The advantage of the multi-plane technique over the generic cylinder element is its higher accuracy and resolution. Therefore, more heat transfer paths and nodes are defined in this method to check the temperature and heat transfer distribution in the machine's various parts, leading to higher complexity and computation time. Moreover, most research studies have implemented the multi-planes approach for low- to middle-range power machines.

Therefore, this paper presents the analytical LPTN of high megawatt machines with an OSV cooling system using the multi-planes technique. The aim is to develop analytical tools for thermal modeling of the OSV electrical machines, focusing on high megawatt synchronous machines with solid salient pole rotors. The research focuses on existing challenges and problems in ongoing method development, and attempts to propose a solution to overcome these challenges. For this purpose, the analytical LPTN by multi-planes technique is developed for a four-pole, two-megawatts synchronous generator with a salient pole rotor with an '*F*' insulation class.

2. Thermal Model Description

Analytical thermal models using multi-planes technique propose three-dimensional (3-D) heat transfer modeling of a machine by developing LPTN in the axial and radial directions. Moreover, this technique attempts to increase the precision and resolution of the thermal model by enhancing the number of nodes and thermal paths; therefore, it consists of a sizable LPTN. In this technique, the machine under investigation is divided into several principal planes. As seen in Figure 1, the machine's active parts are divided into three planes ('A', 'B', and 'C'), and the drive and non-drive machine's end regions are modeled by two other planes ('D' and 'E').

Moreover, as seen in Figure 1, the machine with the OSV cooling system includes several radial cooling ducts in the end section of the stator active part (plane 'C'). Hence, plane 'C' is divided into several sub-plans to model the heat transfer in these sections.

In this technique, each plane consists of a radial thermal model connected to the adjusted planes using interplane resistances, representing the axial thermal model. Furthermore, to develop the analytical thermal model using the multi-planes technique, the below hypotheses have been assumed:

- In the machine under study, the air gap provides the primary airflow path for both stator and rotor; it can be concluded that exchanging heat between the stator and the rotor is negligible, and almost all heat fluxes are transferred to the ambient by the airflow inside air gap. Therefore, it makes it possible to separately model the stator and rotor.
- The heat and heat loss distributions are assumed to be uniform.
- Based on the machine's periodical symmetries, a stator slot and one-quarter of the rotor are analytically modeled.

2.1. Thermal Model in the Radial Direction

Figure 2a,b shows the radial LPTN proposed for the heat transfer modeling of the stator and rotor for the case under study. As seen in Figure 2a, the stator analytical model includes five nodes and eight thermal resistances among the nodes to model the heat transfer in crucial machine parts. Furthermore, in Figure 2b, the rotor radial thermal model includes seven nodes and nineteen thermal resistances. These resistances represent one of the heat transfer phenomena: conduction, convection, and radiation.

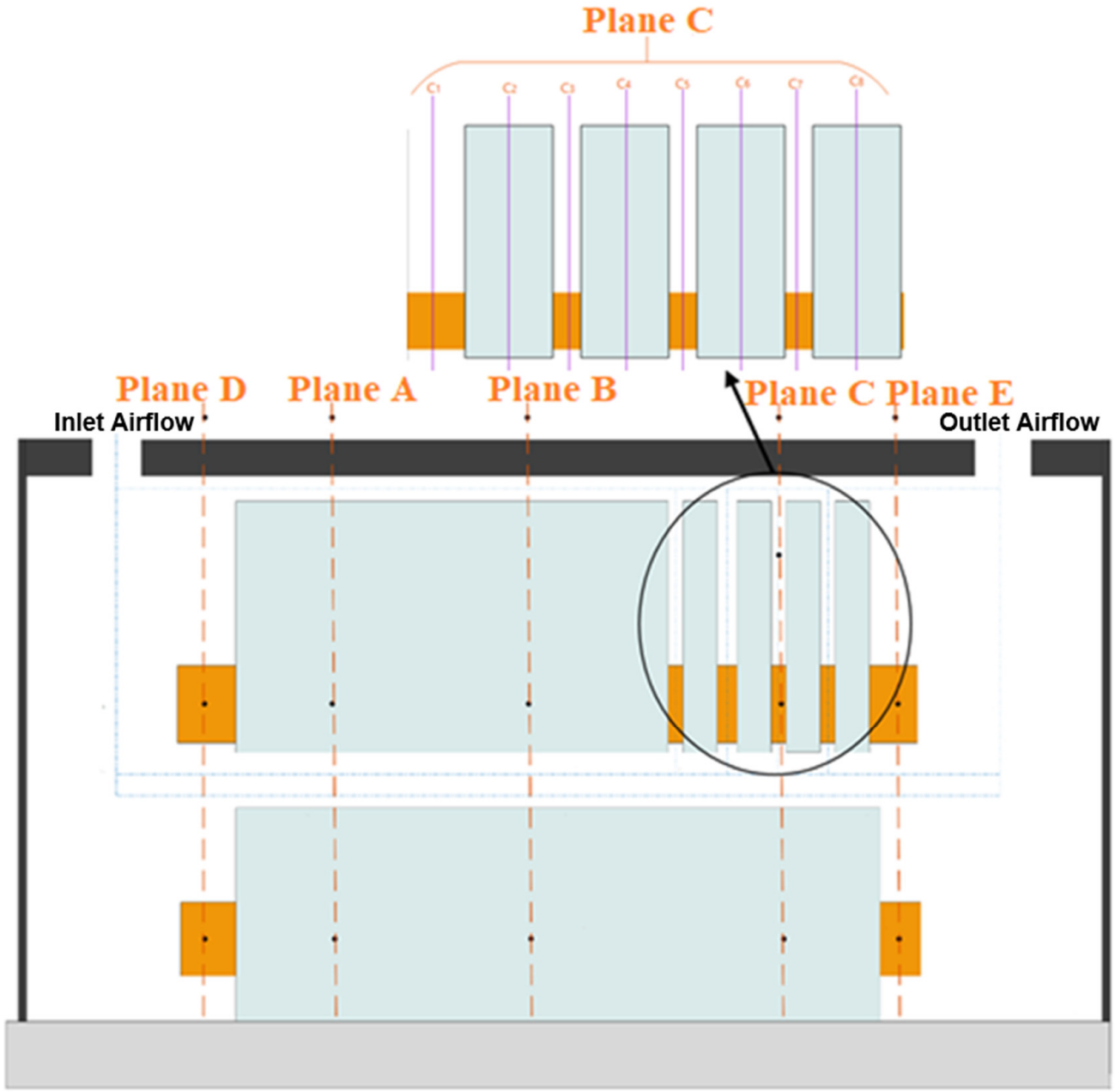

Figure 1. Multiple model plane thermal approach.

2.2. Axial Thermal Model

Figure 3a,b illustrates the axial thermal model or, in other words, the interplane resistances to connect each plane to the adjusted planes for the stator and rotor, respectively. To mitigate complexity and enhance resolution and clarity, for the stator part (Figure 3a), only interplane resistances for the nodal points 0, 1, 4, 5, and 6, and for the rotor (Figure 3b), the nodes 0, 1, 5, and 7, are presented; others are omitted in the figures. Moreover, some other resistances with a blue color are added to the axial LPTN to model the airflow (coolant) temperature rise during the passing of each plane to enhance the precision of the thermal model and estimate the outlet coolant temperature.

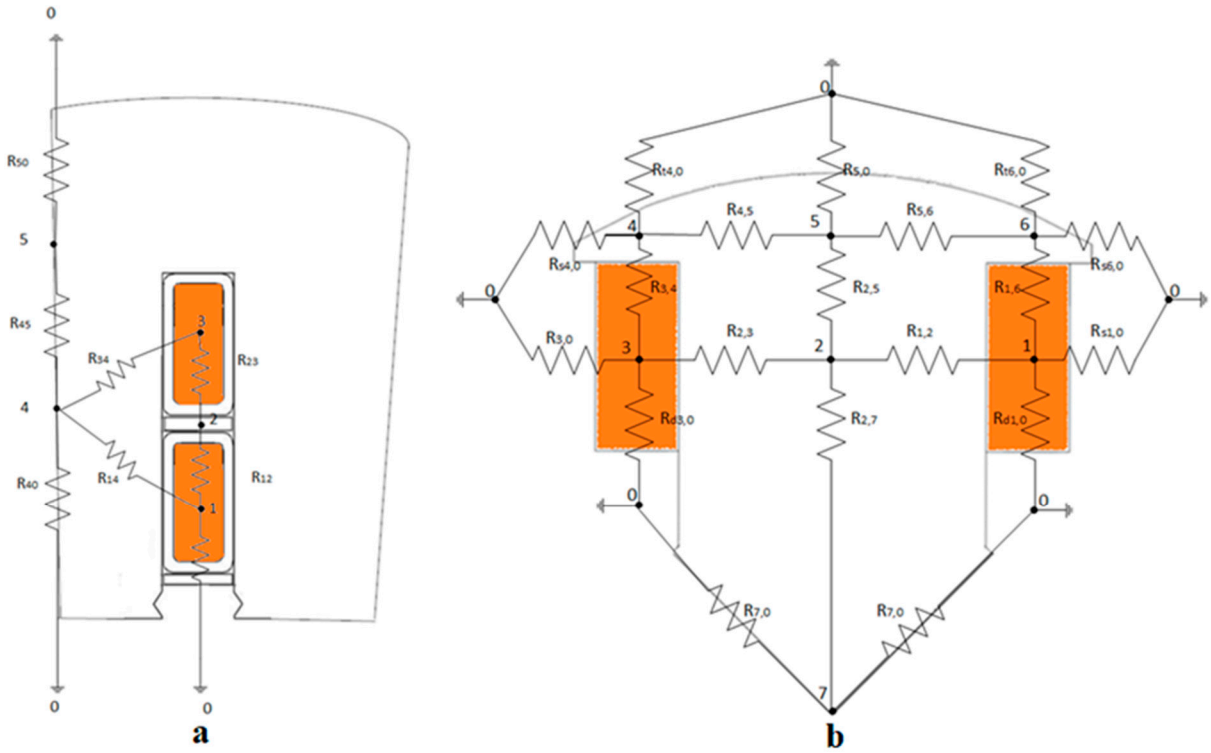

Figure 2. The proposed radial model: (**a**) stator; (**b**) rotor.

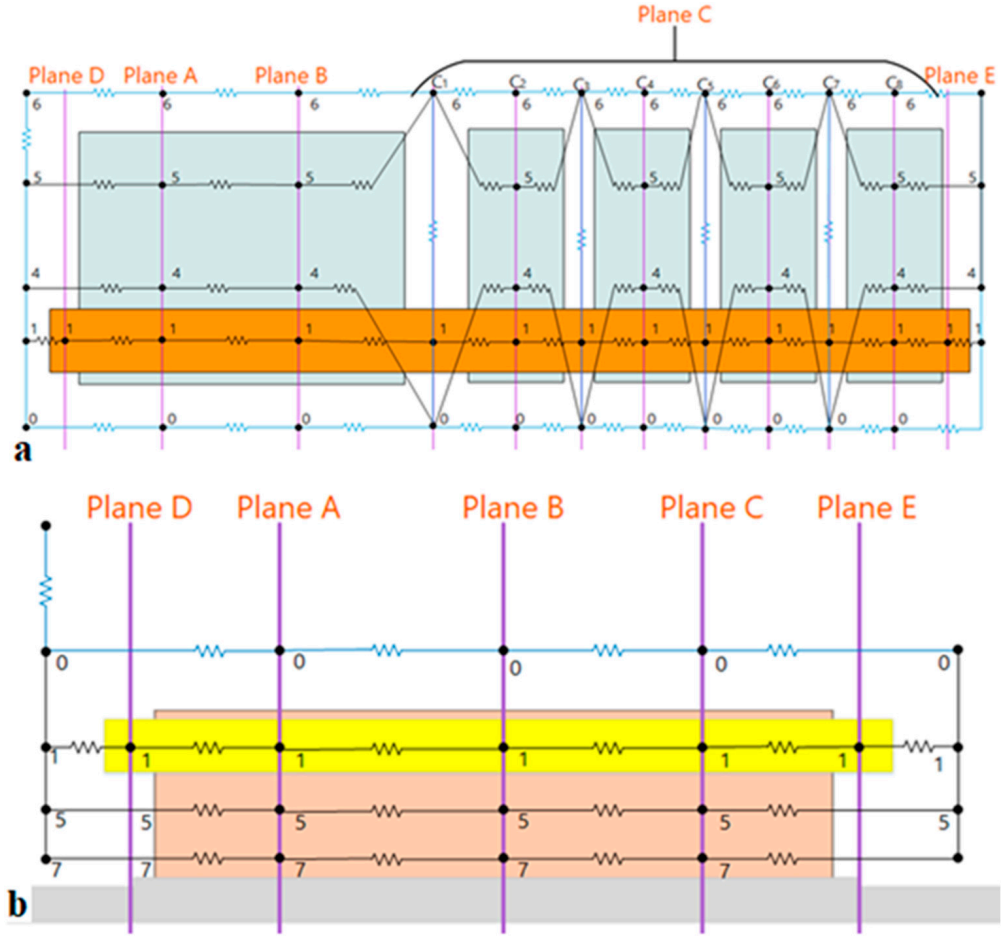

Figure 3. The proposed axial model: (**a**) stator; (**b**) rotor.

3. Determining the Critical Parameters of the Analytical Model

In the heat transfer mechanism, the heat fluxes are transferred by three thermal phenomena: conduction, convection, and radiation [5]. These phenomena are modeled by resistances in the analytical thermal model [18]. Hence, the thermal model's accuracy chiefly depends on the precise estimation of these parameters. However, due to the complex shape of machine parameters, such as end windings, the air gap, and the slot, they cannot be calculated by pure mathematical solutions. Therefore, it is necessary to apply some assumptions and simplifications to reduce the system's complexity and shape to overcome these problems. Hence, this section aims to recognize the crucial parameters during the analytical thermal modeling of OSV machines. As a result, these critical parameters for the machine with an OSV cooling system are classified into two primary groups: critical parameter of conduction heat transfer and critical parameter of convection heat transfer.

3.1. A Critical Parameter of Conduction Heat Transfer

Conduction heat transfer occurs in solid material by transferring the heat fluxes from the hot side to the cold side due to molecular vibration. The general format of correlation to estimate conduction resistance (R_{cond}) is expressed as follows:

$$R_{cond} = \frac{L}{kA}, \tag{1}$$

where L is the conduction length, k represents the material's thermal conductivity, and A is the cross-sectional area.

The most challenging section in the conduction modeling is how to calculate the slot conduction resistance. The slot is composed of several various materials with different thermal conductivities. This section consists of the lowest thermal conductivity in the machine structure, with the highest amount of heat losses by the joule losses. Therefore, accurate slot modeling is essential in thermal analysis and temperature monitoring. Furthermore, most of the materials inside the slot are temperature dependent, and they reduce the lifetime of winding insulation materials and machine life by reaching their temperature threshold.

The most critical part of modeling conduction inside a slot is determining the thermal conductivity of the slot. Several research studies have investigated and proposed various solutions to calculate the thermal conductivity of a slot, such as a layer winding approach [19–22], a cuboidal approach [21,23], an equivalent insulation approach [21], and an equivalent thermal conductivity approach [24,25]. This research study applies the equivalent thermal conductivity approach based on Hashin and Milton's correlation. Hashin and Milton proposed the equivalent thermal conductivity of a slot (k_e), as follows [26,27]:

$$k_e = k_{ins}\frac{(1+f_1)k_{\mathrm{cu}} + (1-f_1)k_{\mathrm{ins}}}{(1-f_1)k_{\mathrm{cu}} + (1+f_1)k_{\mathrm{ins}}}, \tag{2}$$

k_{cu} represents the copper thermal conductivity, k_{ins} equals the thermal conductivity of insulation materials, f_1 and f_2 are the volume fraction of the conductor and the impregnation in the slot, respectively (with $f_1 + f_2 = 1$). The other insulation materials are assumed equivalent to the impregnation material, which is a well-justified assumption, as explained in [26].

3.2. A Critical Parameter of Convection Heat Transfer

During the convection phenomenon, the fluid flow motion exchanges the heat between two different media [28,29]. Therefore, this heat transfer mechanism removes the significant parts of heat. In the analytical calculation, the convection resistance (R_{conv}) is expressed as:

$$R_{conv} = \frac{1}{h_c A}, \tag{3}$$

where h_c is the convection coefficient, and A is the surface area.

According to (3), the most challenging parameter in convection resistance calculation is determining the convection coefficient (h_c). The correct estimation of this factor greatly impacts the accuracy of the thermal model. Therefore, it is mainly calculated using empirical correlations. These correlations have been developed using dimensionless numbers, such as Nusselt (Nu), Prandtl (Pr), and Reynolds (Re) numbers [30] and are primarily defined in the following format:

$$\mathrm{Nu} = a\mathrm{Re}^{b}\mathrm{Pr}^{c}, \tag{4}$$

where a, b, and c are constants.

Ultimately, by calculating the Nusselt number from (4), the convection coefficient is determined as follows [31,32]:

$$h_c = \frac{\mathrm{Nu}.k}{L}, \tag{5}$$

where k is the fluid flow conductivity, and L is the characteristic length of the surface.

The heat is transferred by convection from the stator radial and axial cooling ducts, the air gap, and the end regions for the case under study. The essential empirical correlations to calculate the convection coefficients from the above regions are explained hereafter.

3.2.1. Radial and Axial Stator Cooling Ducts

The axial and radial cooling ducts embedded in the machines are assumed as stationary ducts, and the Nusselt number is calculated using the Gnielinski correlation, which is defined in the following format:

$$\mathrm{Nu_D} = \frac{\left(\frac{f_{smooth}}{8}\right)(\mathrm{Re}-1000)\mathrm{Pr}}{1+12.7\left(\frac{f_{smooth}}{8}\right)^{0.5}\left(\mathrm{Pr}^{0.67}-1\right)}, \tag{6}$$

where f_{smooth} is a friction factor for a smooth wall and is estimated as:

$$f_{smooth} = \frac{1}{\left(1.82\log_{10}\mathrm{Re}-1.64\right)^2}, \tag{7}$$

However, the machine surface is not purely smooth due to the manufacturing process. Therefore, the effect of surface roughness should be applied during the calculation procedure by defining the roughness Nusselt number (Nu_{rough}) as [33]:

$$\frac{\mathrm{Nu}_{rough}}{\mathrm{Nu}_{smooth}} = \left(\frac{f}{f_{smooth}}\right)^{0.68\ \mathrm{Pr}^{0.215}}, \tag{8}$$

3.2.2. Air Gap

For analytical modeling of heat transfer in the air gap, the classical modeling method using the Taylor number (Ta) is most often applied, and it is expressed in the following format [34]:

$$\mathrm{Ta} = \mathrm{Re}\sqrt{\frac{l_g}{r_{or}}}, \tag{9}$$

where l_g is the radial thickness of the air gap, r_{or} is the rotor outer radius.

The flow condition in the air gap (laminar or turbulent) and the Nusselt number are evaluated according to the range of the Taylor number (Ta) as [34]:

$$\begin{cases} \mathrm{Nu} = 2 & \mathrm{Ta} < 41 & \text{laminar mode} \\ \mathrm{Nu} = 0.212\ \mathrm{Ta}^{0.63}\mathrm{Pr}^{0.27} & 41 \le \mathrm{Ta} \le 100 & \text{vortex mode} \\ \mathrm{Nu} = 0.386\ \mathrm{Ta}^{0.5}\mathrm{Pr}^{0.27} & \mathrm{Ta} > 100 & \text{turbulent mode} \end{cases} \tag{10}$$

However, the above correlations cannot be applied for modeling the air gap heat transfer for OSV machines. This is because, unlike other cooling systems, the air gap faces two-fluid flows in OSV machines: the axial flow driven by the fan and the rotational flow due to the rotor rotational speed. This axial flow can positively impact the amount of heat transfer by the convection phenomenon. However, in some cases, it has a negative footprint on the vortices, reducing the heat transfer inside the air gap.

In this manner, the flow condition in the air gap for the machine with an OSV cooling system is classified into four modes as follows [35]:

- Laminar flow;
- Turbulent flow;
- Laminar flow with Taylor Vortices;
- Turbulent flow with Taylor Vortices.

Thus, the correlations presented in Table 1 assess the heat transfer coefficient according to the fluid modes.

Table 1. Correlations for computing the air gap convection coefficient [35,36].

Flow Modes	Empirical Correlation	Ref
Laminar	$\mathrm{Nu} = 7.54 + \frac{0.03\left(\frac{D_h}{L}\right)\mathrm{RePr}}{1+0.016\left[\left(\frac{D_h}{L}\right)\mathrm{RePr}\right]^{2/3}}$	[37]
Turbulent	$\mathrm{Nu_D} = \frac{\left(\frac{f_{smooth}}{8}\right)(\mathrm{Re}-1000)\mathrm{Pr}}{1+12.7\left(\frac{f_{smooth}}{8}\right)^{0.5}\left(\mathrm{Pr}^{0.67}-1\right)}$	[35]
Laminar with Taylor Vortices	$\mathrm{Nu} = \mathrm{Nu_{axial}} + \mathrm{Nu_{rotational}}$ $\mathrm{Nu_{axial}} = 0.015\left(1+4.6\frac{s}{L}\right)\left(\frac{r_i}{r_O}\right)^{0.45}\mathrm{Re}^{0.8}\mathrm{Pr}^{1/3}$ $\mathrm{Nu_{rotational}} = 0.092\left(\mathrm{Ta}^2\mathrm{Pr}\right)^{1/3}$	[38]
Turbulent with Taylor Vortices	$V_e = \sqrt{U^2 + \left(\frac{V_T}{2}\right)^2}$ $\mathrm{Nu} = 0.03\left(\frac{D_h V_e}{v}\right)^{0.8}$	[39]

3.2.3. End Regions

End regions count as the most challenging parts of analytical thermal modeling. Therefore, this section comprises several parts that can be classified into five primary sections: inner housing surfaces, stator teeth and yoke, end windings, rotor steels and end rings, and shaft.

1. End Windings

The end windings are one of the challenging features of machine thermal modeling. The end windings are cooled in the OSV machine by the radial and axial airflows generated by the rotor end parts and the fan. For a high megawatt machine, the form-wound configuration is mainly applied. As seen in Figure 4, contrary to conventional round wires, the gaps among the end-windings are not filled by impregnation material in the form-wound configuration. Hence, the conductors are in direct contact with the coolant. Therefore, the convection coefficient of the end windings is not estimated by the traditional correlation presented in [35,36]. Instead, the Churchill and Bernstein correlation [37], applied for the cylinder in cross-flow, is utilized to overcome the problem. In this condition, the Nusselt number is defined as:

$$\mathrm{Nu} = 0.3 + \frac{0.62\mathrm{Re}^{0.5}\mathrm{Pr}^{0.33}}{\left[1+\left(\frac{0.4}{\mathrm{Pr}}\right)^{0.67}\right]^{0.25}}\left[1+\left(\frac{\mathrm{Re}}{282000}\right)^{0.625}\right]^{0.8}. \quad (11)$$

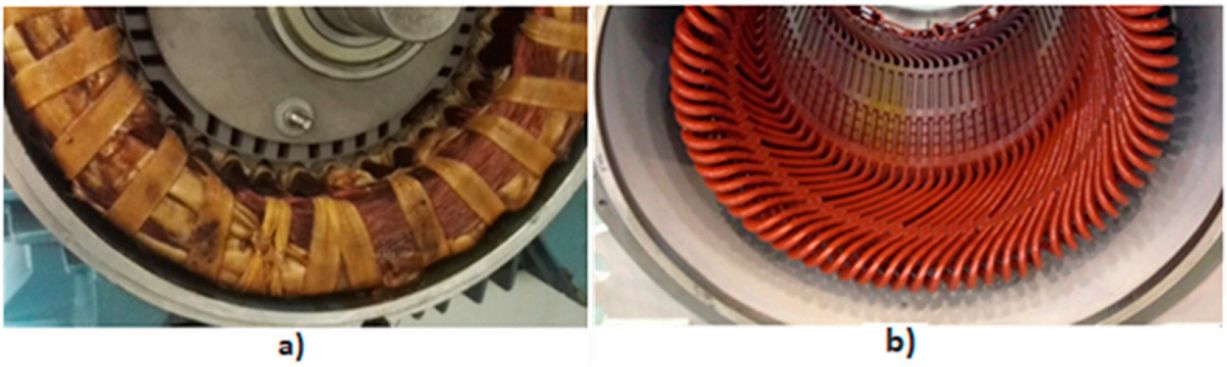

Figure 4. End windings: (**a**) conventional strand configuration, (**b**) form-wound configuration [5].

2. Yoke and stator teeth

The yoke and stator teeth are assumed to be flat non-rotational surfaces in a machine end region. Depending on their location and their condition in contact with axial airflow, two sets of empirical correlations are defined for calculating the Nusselt number for inlet and outlet non-rotational surfaces, respectively, as [40,41]:

$$\mathrm{Nu} = 0.592\ \mathrm{Re}^{0.5}, \tag{12}$$

$$\mathrm{Nu} = 0.17\ \mathrm{Re}^{0.67}. \tag{13}$$

3. Rotor steels and end rings

The rotor steel and end rings are considered flat rotational surfaces, and the Nusselt number in this manner is defined as [40,41]:

$$\mathrm{Nu} = 0.28973\left(\mathrm{Re}_a^2 + \mathrm{Re}_{rot}^2\right)^{0.25}, \tag{14}$$

This correlation involves the impact of axial and rotor rotation airflow by defining two sets of Reynolds numbers represented by the axial airflow (Re_a) and rotor rotation airflow (Re_{rot}), which are respectively defined as [40,41]:

$$\mathrm{Re}_a = \frac{v_{air} D}{\mu}, \tag{15}$$

$$\mathrm{Re}_{rot} = \frac{\omega_{rot} D^2}{4\mu}, \tag{16}$$

where v_{air} is the axial airflow rate, ω_{rot} is the rotor angular speed, D is the hydraulic diameter, and μ is the dynamic viscosity of the airflow.

The critical point is in the inlet; both Reynolds numbers are calculated. However, only rotor rotational Reynold numbers are computed in the outlet section, and the other one is omitted as $v_{air} = 0$.

4. Inner housing surfaces

The machine's inner housing, located in the end region, is considered a cylindrical non-rotational surface. Therefore, the Nusselt number correlation is the same utilized for smooth surface ducts.

5. Shaft

The parts of the shaft located in the machine's end region are considered cylindrical rotational surfaces, and the Nusselt number is defined as [40,41]:

$$\mathrm{Nu} = 0.6366\ (\mathrm{Re}_{rot}\mathrm{Pr})^{0.5}. \tag{17}$$

3.3. Modeling the Coolant Flow

There are various techniques by which to model the coolant flow. Generally, in the electrical machine's thermal model with an enclosed cooling system, such as a totally enclosed fan-cooled system, coolant temperature is assumed to be constant [42]. Therefore, using this hypothesis in the model provides good accurate temperature results. However, contrary to the enclosed cooling system, an electric machine consists of an open-circuit cooling system in OSV or through the ventilation cooling method; the coolant temperature rise is significant [42]. Therefore, using the constant coolant temperature hypothesis leads to a significant error in the final temperature results of the thermal model [42,43]. Hence, predicting and modeling the coolant temperature in the machine's different parts plays an essential role in the LPTN's accuracy [12].

In this method, the coolant network is developed to match the thermal network to reduce computational complexity [43]. Figure 5 shows the stator coolant network; this coolant network consists of 16 points by which to model the airflow paths. Accordingly, the coolant enters from the inlet and gathers in node 1. Then, the coolant flow segregates into two parts; one flows through the stator axial channels (node 2), and the other flows from the air gap (node 3). According to the multi-planes approach, various nodes are set to model the absorbed losses by coolant over passing planes. This process continues until plane 'C'. Plane 'C' is divided into several sub-planes to increase the resolution and match the coolant network with the thermal model. Hence, the number of nodes rapidly increases and follows the number of sub-planes.

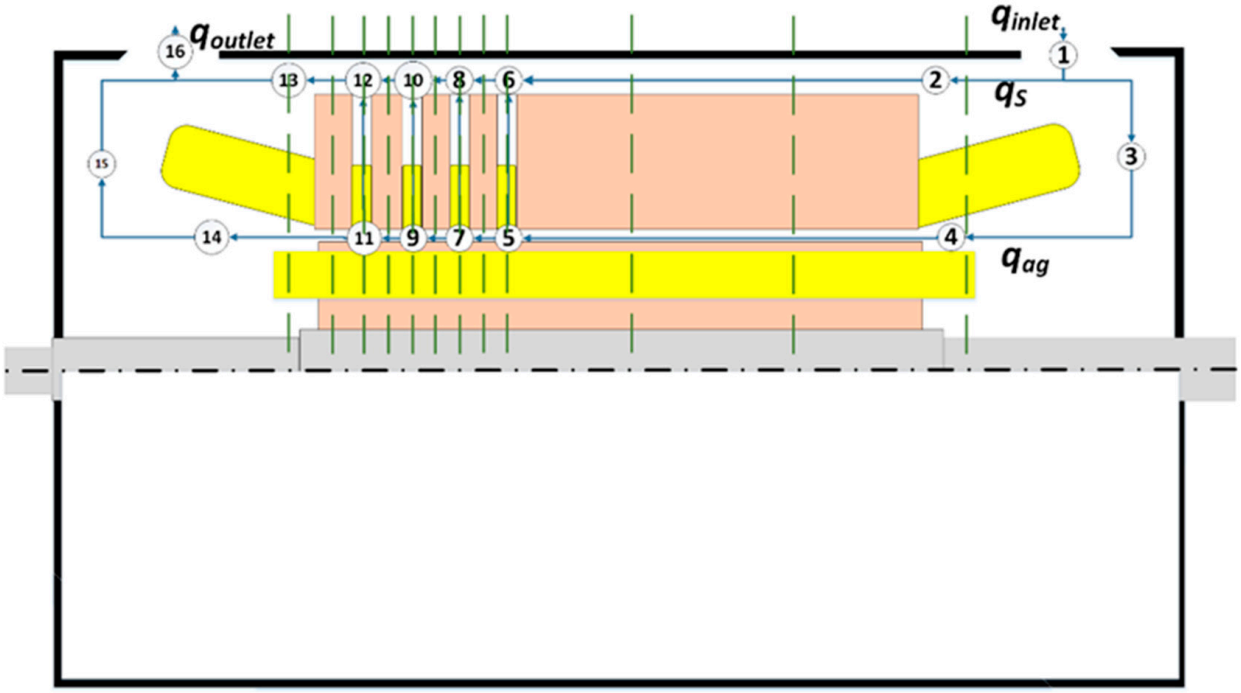

Figure 5. Stator's coolant network.

Figure 6 shows the rotor's coolant network and the coolant temperature rising diagram over passing planes to provide a holistic view of the coolant temperature growing process. In this approach, the coolant temperature rising by absorbing the heat losses is linearly hypothesized over the planes.

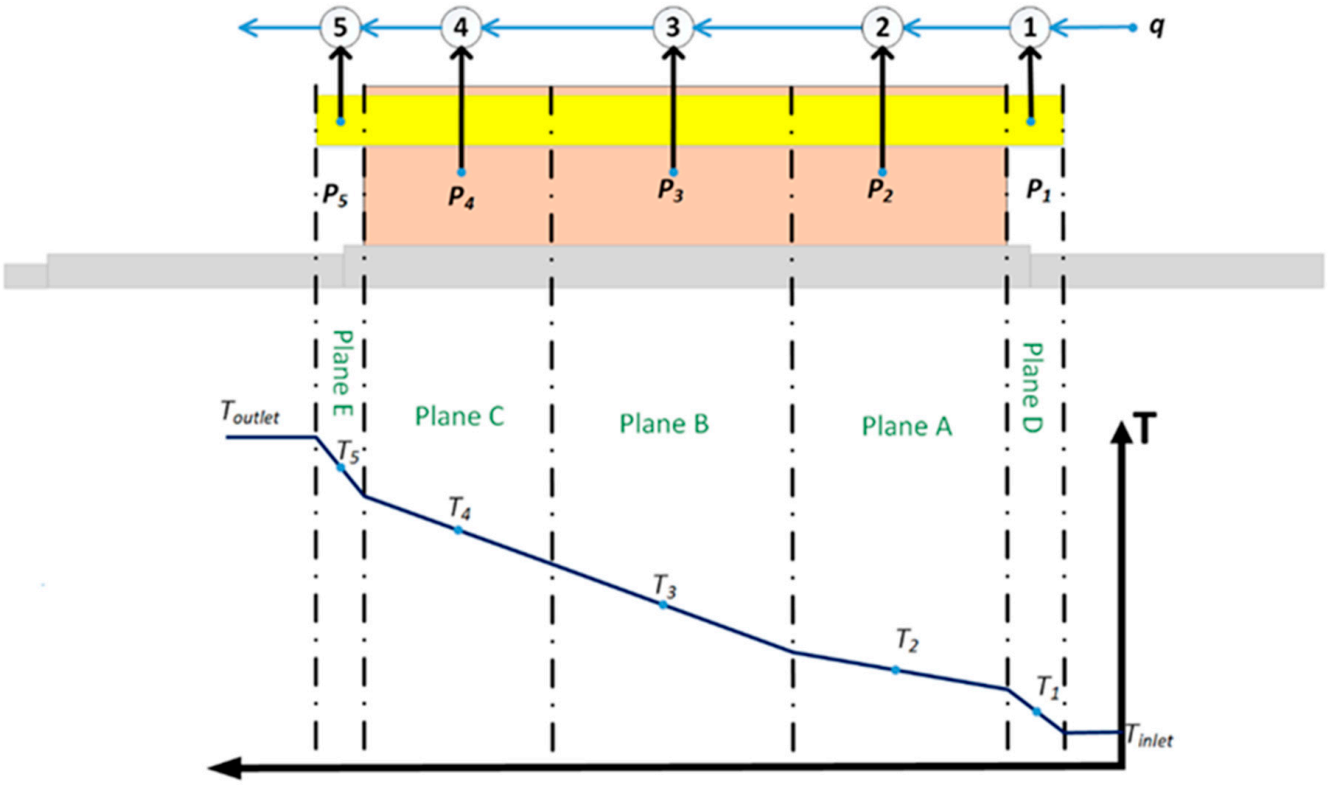

Figure 6. Rotor's coolant network and its temperature rising diagram.

The coolant and thermal networks are coupled to implement the effect of a coolant temperature rise. Therefore, the coolant flow path is added to the thermal model by the blue color resistances. As a result, the coolant flow resistance is estimated as follows [12]:

$$R_q = \frac{1}{\rho q c_p}, \tag{18}$$

where ρ is mass density, c_p is the coolant-specific heat, and q is the volume of the flow rate of coolant.

4. Analytical Computation Approach

The generic MATLAB code is developed to couple the thermal model and coolant network. Figure 7 shows and describes the various code's steps in detail. The first step reads the input parameters consisting of the machine's dimensions, initial values, and material thermal properties. Then, the variable parameters such as rotor speed and coolant thermal characteristics are calculated. Next, conduction resistances in the radial and axial directions for the stator and rotor are calculated and assigned to the LPTN model presented in sections II and III. The convection coefficients are determined according to the analytical hydraulic analysis values in step six. Then, the convective resistances are computed through the model presented in sections II and III. In step 7, the coolant network's resistances are calculated, and, in step 8, the heat sources are defined as the current sources and injected into the corresponding nodes. Finally, the conductance matrix, fluid matrices, and loss matrix are developed, and the matrices' models are solved by inversion theory. The generation of the conductance, fluid, and loss matrices and the matric inversion solving method are described here.

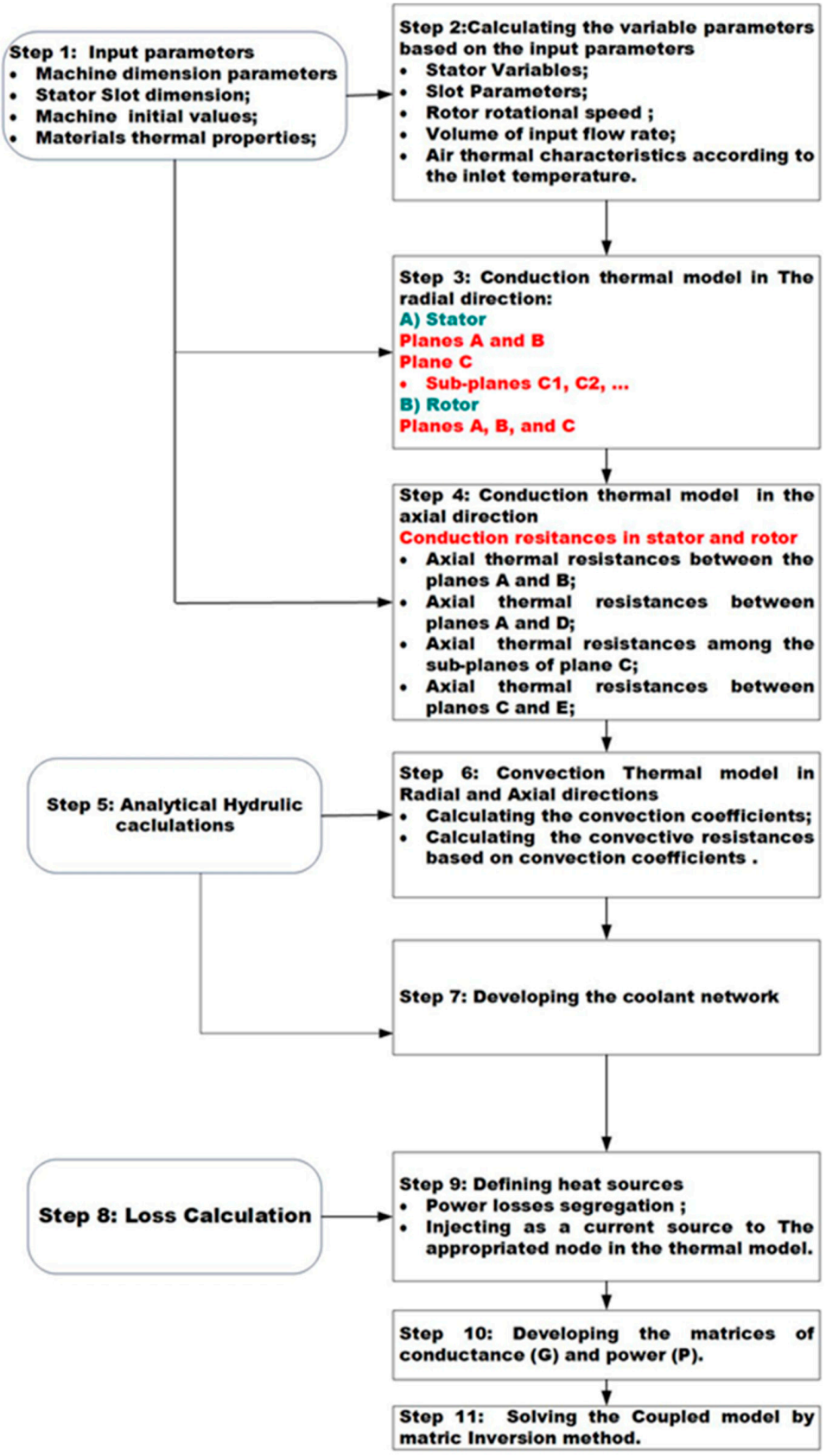

Figure 7. The flow chart and code algorithm of the multi-plane thermal model.

In the analytical model analysis, the temperature matrix containing the temperature of each node (**T**) is calculated utilizing the Matrix inversion technique, as follows [11]:

$$\mathbf{T} = (\mathbf{G} + \mathbf{G_{fluid}})^{-1}\mathbf{P} \tag{19}$$

where **G** and $\mathbf{G_{fluid}}$ are the thermal conductance and cooling matrices, respectively, and **P** is the loss vector containing the power losses of each node. Moreover, the thermal conductance (**G**) and cooling ($\mathbf{G_{fluid}}$) as squared matrices are developed in the following formats, respectively [12,44]:

$$\mathbf{G} = \begin{bmatrix} \sum_{i=1}^{n} \frac{1}{R_{1,i}} & -\frac{1}{R_{1,2}} & \cdots & -\frac{1}{R_{1,n}} \\ -\frac{1}{R_{2,1}} & \sum_{i=1}^{n} \frac{1}{R_{2,i}} & \cdots & -\frac{1}{R_{2,n}} \\ \vdots & \vdots & \ddots & \vdots \\ -\frac{1}{R_{n,1}} & -\frac{1}{R_{n,1}} & \cdots & \sum_{i=1}^{n} \frac{1}{R_{n,i}} \end{bmatrix}, \tag{20}$$

$$\mathbf{G_{fluid}} = \begin{bmatrix} \sum_{i=1}^{n} \frac{1}{R_{q1,i}} & 0 & \cdots & 0 \\ -\frac{1}{R_{q2,1}} & \sum_{i=1}^{n} \frac{1}{R_{q2,i}} & \cdots & -\frac{1}{R_{q2,n}} \\ \vdots & \vdots & \ddots & \vdots \\ -\frac{1}{R_{qn,1}} & -\frac{1}{R_{qn,1}} & \cdots & \sum_{i=1}^{n} \frac{1}{R_{qn,i}} \end{bmatrix}, \tag{21}$$

5. Determining the Analytical Thermal Model Performance

5.1. Experimental Setup

An experimental verification stage was carried out to validate the created analytical model and obtain details about the method's accuracy in estimating the nodal temperature machine's key parameters. For this purpose, the analytical and experimental results for the OSV AM 0560AF04 DAP synchronous machine, designed and constructed for wind generator applications, are compared. Table 2 shows the nominal values of the machine.

Table 2. Rated values of the tested synchronous machine.

Parameter	Unite	Value
Rated Power	kVA	2001
Rated Frequency	Hz	50
Rated Voltage	kV	11
Rated Current	A	105

For this purpose, the machine underwent runs at the rated load and frequency. The machine consists of the form winding configuration with an "*F*" insulation class. In addition, RTD PT100 sensors equip the tested motor to record the temperatures of specific parts of the machine, such as windings, inlet and outlet air, and ambient temperature.

5.2. Comparison of Analytical and Experimental Data

Table 3 presents the analysis of the analytical model using the multi-planes technique at rated load and frequency. As expected, the hottest point is in the end windings of the machine located at plane 'E' with a temperature of 112.5 (°C). In this area, the airflow temperature as a coolant is approximately 41 (°C), about 10 degrees more than the inlet coolant temperature. Moreover, the analytical results show the lowest temperature in Plane 'A'.

Table 3. Analytical results of the thermal model.

Node's Location	Temperature (°C)
Stator end winds located in-plane 'D'	107.1
Stator winding in plane 'B'	105.7
Stator end windings located in-plane 'E'	112.5
Stator yoke in-plane 'A'	97.4
Upperside of stator slot in-plane 'A'	106.8
Middle of stator slot in-plane 'B'	103.6
Downside of stator slot in-plane 'A'	100.4
Stator teeth temperature in-plane 'A'	98.8
Outlet coolant	41.1

The machine was run under its rate speed (1500-rpm) and at full load during the experiment. Moreover, the inlet airflow, ambient and winding temperatures, and volumetric cooling airflow rate were measured. Accordingly, the airflow temperature in the inlet section and ambient temperature were 32 (°C) and 28.3 (°C), respectively. Furthermore, the volumetric cooling air flow rate was 3.7 (m^3/s). Table 4 presents the analytical and measurement data for the stator winding and the outlet coolant. It is important to mention that the stator winding temperature is the mean temperature of three-phase windings. The deviation between the analytical and experimental results was above 1%, and there was good agreement between the analytical and measurement data.

Table 4. Analytical and measurement data.

Name of Section	Analytical Data (°C)	Measurement Data (°C)
Stator Windings	103.6	104.8
Outlet Coolant	41.1	42.9

6. Conclusions

This paper investigated the thermal modeling of a synchronous generator with a salient pole rotor for a high-power application. Therefore, the analytical LPTN using the multi-planes method was proposed as an ideal method by which to develop the thermal analysis tools to model the heat transfer of the machine to achieve the objectives established. First, the fundamental principles of the heat transfer mechanism were explained, and prevalent correlations and challenging factors in the thermal analysis were represented. Moreover, different methods by which to overcome these challenges were demonstrated. Furthermore, the principle of the coolant network and the way to couple it with the thermal network were discussed in detail. Different methods were described to consider the effect of the coolant temperature rising, and the best option to model the coolant temperature rising for the OSV system was introduced. According to the results, the difference between the inlet and outlet coolant temperatures was about 9 (°C), and it had a great impact on the final nodal temperature; implementing this impact on the thermal analysis was essential.

Finally, the experiment was conducted to validate the analytical thermal model based on the multi-plane's technique. Obtained analytical and experimental data were in good agreement. Therefore, the analytical model was successfully applied to estimate the machine temperature distribution, and the temperature difference between the analytical and experimental data was about 1%.

Author Contributions: Conceptualization, P.S.G., A.P., A.K., A.B. and A.J.M.C.; methodology, P.S.G., A.P. and A.K.; validation, P.S.G. and A.K.; data curation, P.S.G.; writing—original draft preparation, P.S.G.; writing—review and editing, A.J.M.C., A.B., B.A., M.N.I. and T.V.; visualization, O.K. and T.V.; supervision, A.P. All authors have read and agreed to the published version of the manuscript.

Funding: This work has been supported by the European Regional Development Fund within the Activity 1.1.1.2 "Postdoctoral Research Aid" of the Specific Aid Objective 1.1.1 "To increase the research and innovative capacity of scientific institutions of Latvia and the ability to attract external financing, investing in human resources and infrastructure" of the Operational Programme "Growth and Employment" (No.1.1.1.2/VIAA/3/19/501).

Data Availability Statement: Not applicable.

Conflicts of Interest: The authors declare no conflict of interest.

References

1. Shams Ghahfarokhi, P.; Kallaste, A.; Podgornov, A.; Belahcen, A.; Vaimann, T.; Kudrjavtsev, O. Thermal analysis of salient pole synchronous machines by multiple model planes approach. In Proceedings of the 2020 International Conference on Electrical Machines, Gothenburg, Sweden, 23–26 August 2020; pp. 1511–1517.
2. Boglietti, A.; Cavagnino, A.; Staton, D.; Shanel, M.; Mueller, M.; Mejuto, C. Evolution and Modern Approaches for Thermal Analysis of Electrical Machines. *IEEE Trans. Ind. Electron.* **2009**, *56*, 871–882. [CrossRef]
3. Mejuto, C. *Improved Lumped Parameter Thermal Modelling of Synchronous Generators*; The University of Edinburgh: Edinburgh, UK, 2010.
4. Micallef, C. End Winding Cooling in Electric Machines. Ph.D. Thesis, University of Nottingham, Nottingham, UK, 2006; pp. 1–193.
5. Shams Ghahfarokhi, P.; Kallaste, A.; Belahcen, A.; Vaimann, T. Analytical thermal model and flow network analysis suitable for open self-ventilated machines. *IET Electr. Power Appl.* **2020**, *14*, 929–936. [CrossRef]
6. Boglietti, A.; Cavagnino, A.; Staton, D. Determination of Critical Parameters in Electrical Machine Thermal Models. *IEEE Trans. Ind. Appl.* **2008**, *44*, 1150–1159. [CrossRef]
7. Nategl, S.; Lindberg, D.; Aglen, O.; Brammer, R.; Boglietti, A. Review and Trends in Traction Motor Design: Electromagnetic and Cooling System Layouts. In Proceedings of the 2018 23rd International Conference on Electrical Machines, ICEM 2018, Alexandroupoli, Greece, 3–6 September 2018; pp. 2600–2606.
8. Boglietti, A.; Nategh, S.; Carpaneto, E.; Boscaglia, L.; Scema, C. An optimization method for cooling system design of traction motors. In Proceedings of the 2019 IEEE International Electric Machines and Drives Conference, IEMDC 2019, San Diego, CA, USA, 12–15 May 2019; pp. 1210–1215.
9. Scema, C.; Nategh, S.; Boglietti, A.; Boscaglia, L.; Ericsson, D. A hybrid thermal modeling method for traction motors used in duty-cycles. In Proceedings of the 2019 IEEE International Electric Machines and Drives Conference, IEMDC 2019, San Diego, CA, USA, 12–15 May 2019; pp. 2132–2137.
10. Traxler-Samek, G.; Zickermann, R.; Schwery, A. Cooling airflow, losses, and temperatures in large air-cooled synchronous machines. *IEEE Trans. Ind. Electron.* **2009**, *57*, 172–180. [CrossRef]
11. de Legarra, M.S. *Thermal and Hydraulic Design of Water-Based Cooling Systems for Electrical Machines*; University of Navarra: Pamplona, Spain, 2017.
12. Nerg, J.; Ruuskanen, V. Lumped-parameter-based thermal analysis of a doubly radial forced-air-cooled direct-driven permanent magnet wind generator. *Math. Comput. Simul.* **2013**, *90*, 218–229. [CrossRef]
13. Nerg, J.; Rilla, M.; Pyrhönen, J. Thermal analysis of radial-flux electrical machines with a high power density. *IEEE Trans. Ind. Electron.* **2008**, *55*, 3543–3554. [CrossRef]
14. Malumbres, J.A.; Satrustegui, M.; Elosegui, I.; Ramos, J.C.; Martínez-Iturralde, M. Analysis of relevant aspects of thermal and hydraulic modeling of electric machines. Application in an Open Self Ventilated machine. *Appl. Therm. Eng.* **2015**, *75*, 277–288. [CrossRef]
15. Mellor, P.H.; Roberts, D.; Turner, D.R. Lumped parameter thermal model for electrical machines of TEFC design. *IEE Proc. B Electr. Power Appl.* **1991**, *138*, 205. [CrossRef]
16. Mejuto, C.; Mueller, M.; Shanel, M.; Mebarki, A.; Reekie, M.; Staton, D. Improved synchronous machine thermal modelling. In Proceedings of the 2008 18th IEEE International Conference on Electrical Machine (ICEM), Vilamoura, Portugal, 6–9 September 2008.
17. Mejuto, C.; Mueller, M.; Shanel, M.; Mebarki, A.; Staton, D. Thermal modelling investigation of heat paths due to iron losses in synchronous machines. In *IET Conference Publications*; Institution of Engineering and Technology (IET): Prague, Czech Republic, 2008; pp. 225–229.
18. Shams Ghahfarokhi, P.; Kallaste, A.; Vaimann, T.; Belahcen, A. Thermal Analysis of Totally Enclosed Fan Cooled Synchronous Reluctance Motor-state of art—IEEE Conference Publication. In Proceedings of the IECON 2019—45th Annual Conference of the IEEE Industrial Electronics Society, Lisbon, Portugal, 14–17 October 2019; pp. 1–5.
19. Nategh, S.; Wallmark, O.; Leksell, M.; Zhao, S. Thermal analysis of a PMaSRM using partial FEA and lumped parameter modeling. *IEEE Trans. Energy Convers.* **2012**, *27*, 477–488. [CrossRef]
20. Nategh, S. *Thermal Analysis and Management of High-Performance Electrical Machines*; KTH: Stockholm, Sweden, 2013.
21. Boglietti, A.; Carpaneto, E.; Cossale, M.; Vaschetto, S.; Popescu, M.; Staton, D.A. Stator winding thermal conductivity evaluation: An industrial production assessment. *IEEE Trans. Ind. Appl.* **2016**, *52*, 3893–3900. [CrossRef]
22. Motor-CAD Software by Motor Design—EMag, Therm and Lab. Available online: https://www.motor-design.com/motor-cad-software/ (accessed on 14 August 2020).

23. Wrobel, R.; Mellor, P.H. A general cuboidal element for three-dimensional thermal modelling. *IEEE Trans. Magn.* **2010**, *46*, 3197–3200. [CrossRef]
24. Pyrhönen, J.; Jokinen, T.; Hrabovcová, V. *Design of Rotating Electrical Machines*; Wiley: Hoboken, NJ, USA, 2008.
25. Rosu, M.; Zhou, P.; Lin, D.; Ionel, D.M.; Popescu, M.; Blaabjerg, F.; Staton, D. *Multiphysics Simulation by Design for Electrical Machines, Power Electronics and Drives*, 1st ed.; Wiley-IEEE Press: New York, NY, USA, 2017.
26. Popescu, M.; Staton, D.; Dorrell, D.; Marignetti, F.; Hawkins, D. Study of the thermal aspects in brushless permanent magnet machines performance. In Proceedings of the 2013 IEEE Workshop on Electrical Machines Design, Control and Diagnosis (WEMDCD), Paris, France, 11–12 March 2013; pp. 60–69.
27. Shams Ghahfarokhi, P.; Kallaste, A.; Belahcen, A.; Vaimann, T.; Rassõlkin, A. Hybrid thermal model of a synchronous reluctance machine. *Case Stud. Therm. Eng.* **2018**, *12*, 381–389. [CrossRef]
28. Shams Ghahfarokhi, P.; Kallaste, A.; Vaimann, T.; Rassolkin, A.; Belahcen, A. Determination of forced convection coefficient over a flat side of coil. In Proceedings of the 2017 IEEE 58th International Scientific Conference on Power and Electrical Engineering of Riga Technical University (RTUCON), Riga, Latvia, 12–13 October 2017; pp. 1–4.
29. Ghahfarokhi, P.S.; Belahcen, A.; Kallaste, A.; Vaimann, T.; Gerokov, L.; Rassolkin, A. Thermal Analysis of a SynRM Using a Thermal Network and a Hybrid Model. In Proceedings of the 2018 XIII International Conference on Electrical Machines (ICEM), Alexandroupoli, Greece, 3–6 September 2018; pp. 2682–2688.
30. Gai, Y.; Kimiabeigi, M.; Chuan Chong, Y.; Widmer, J.; Deng, X.; Popescu, M.; Goss, J.; Staton, D.; Steven, A. Cooling of Automotive Traction Motors: Schemes, Examples, and Computation Methods. *IEEE Trans. Ind. Electron.* **2019**, *66*, 1681–1692. [CrossRef]
31. Shams Ghahfarokhi, P.; Kallaste, A.; Vaimann, T.; Rassolkin, A.; Belahcen, A. Determination of natural convection heat transfer coefficient over the fin side of a coil system. *Int. J. Heat Mass Transf.* **2018**, *126*, 677–682. [CrossRef]
32. Shams Ghahfarokhi, P.; Kallaste, A.; Vaimann, T.; Belahcen, A. Natural convection from flat side's of coil system. In Proceedings of the 2018 19th International Scientific Conference on Electric Power Engineering (EPE), Brno, Czech Republic, 16–18 May 2018; pp. 1–5.
33. Stimpson, C.K.; Snyder, J.C.; Thole, K.A.; Mongillo, D. Roughness effects on flow and heat transfer for additively manufactured channels. *J. Turbomach.* **2016**, *138*, 5. [CrossRef]
34. Staton, D.; Boglietti, A.; Cavagnino, A. Solving the More Difficult Aspects of Electric Motor Thermal Analysis in Small and Medium Size Industrial Induction Motors. *IEEE Trans. Energy Convers.* **2005**, *20*, 620–628. [CrossRef]
35. Chong, Y.C.; Goss, J.; Popescu, M.; Staton, D.; Hawkins, D.; Boglietti, A. Electromagnetic performance with and without considering the impact of rotation on convective cooling. *J. Eng.* **2019**, *17*, 3537–3541. [CrossRef]
36. Chong, Y.C. *Thermal Analysis and Air Flow Modelling of Electrical Machines*; The University of Edinburgh: Edinburgh, UK, 2015.
37. Mills, A.F. *Heat Transfer*; Prentice Hall: Hoboken, NJ, USA, 1999.
38. Tachibana, F.; Fukui, S. Convective Heat Transfer of the Rotational and Axial Flow between Two Concentric Cylinders. *Bull. JSME* **1964**, *7*, 385–391. [CrossRef]
39. Gazley, C. Heat transfer characteristics of the rotational and axial flow between concentric cylinders. *J. Heat Transf.* **1958**, *80*, 79–90. [CrossRef]
40. Malumbres, J.A.; Satrustegui, M.; Elosegui, I.; Martínez-Iturralde, M. Coupled thermal and hydraulic algebraic models for an open self-ventilated induction machine. *IET Electr. Power Appl.* **2015**, *9*, 513–522. [CrossRef]
41. Cheng, W.T.; Lin, H.T. Unsteady and steady mass transfer by laminar forced flow against a rotating disk. *Wärme-Und Stoffübertragung* **1994**, *30*, 101–108. [CrossRef]
42. Jokinen, T.; Saari, J. Modelling of the coolant flow with heat flow controlled temperature sources in thermal networks. *IEE Proc. Electr. Power Appl.* **1997**, *144*, 338–342. [CrossRef]
43. Kauh, S.K.; Hahn, S.; Lee, Y. Thermal analysis of induction motor with forced cooling channels. *IEEE Trans. Magn.* **2000**, *36*, 1398–1402. [CrossRef]
44. Shams Ghahfarokhi, P.; Kallaste, A.; Vaimann, T.; Rassolkin, A.; Belahcen, A. Steady-state thermal model of a synchronous reluctance motor. In Proceedings of the 2018 IEEE 59th Annual International Scientific Conference on Power and Electrical Engineering of Riga Technical University, RTUCON 2018, Riga, Latvia, 12–13 November 2018.